Modeling of Hysteretic Behavior of Soil–Water Retention Curves Using an Original Pore Network Model

Harifidy Ranaivomanana, Geetanjali Das, Andry Razakamanantsoa

Modeling of hysteretic behavior of soil-water retention curves using an original pore network model.

Harifidy Ranaivomanana[a,*], Geetanjali Das[b], Andry Razakamanantsoa[b]

[a]: University of Nantes – IUT Saint-Nazaire, GeM, CNRS UMR 6183, Research Institute in Civil Engineering and Mechanics, 58 rue Michel Ange (BP 420), 44606 Saint Nazaire Cedex, France

[b]: Université Gustave Eiffel, Laboratoire GERS-GIE, F-44344 Bouguenais, France

**corresponding author: harifidy.ranaivomanana@univ-nantes.fr, https://orcid.org/0000-0002-9641-5846*

Declarations

***Funding*:** This research received no specific grant from any funding agency in the public, commercial, or not-for-profit sectors.

***Conflicts of interest/Competing interests*:** The authors declare that they have no known competing financial interests or personal relationships that could have appeared to influence the work reported in this paper.

***Availability of Data and Material*:** The authors confirm that the data supporting the findings of this study are available within the article (measured by the authors or extracted from their respective published source in the literature that is listed in the reference section).

Code availability: The model was implemented via the free software SCILAB using simple numerical procedures described in the work.

Abstract

Soil Water Retention Curve (SRWC), also called soil moisture characteristic, is used for simulation models of soil water storage or soil aggregate stability. The present study addresses the modeling of SRWC with particular attention paid to hysteresis effects of water filling and draining the pores attributed to ink-bottle effects. For that purpose, an idealized pore size distribution previously developed for predicting water

sorption isotherms on cementitious materials, and which can consider the double porosity structure of soils, is used. An inverse analysis performed on experimental results of SRWC obtained on different types of soils has allowed to propose a calibration method of parameters involved in the definition of the idealized pore size distribution that can be assessed from mercury intrusion porosimetry tests (MIP) and from grain size distribution (GSD). The model adequately reproduces the hysteretic behavior of SRWC and can also predict the specific surface area.

Keywords: Soil, Water retention Curve; hysteresis; modeling; pore size distribution

Article highlights

- The water retention properties of soils are predicted basing on an original representation of the pore structure.
- Geometrical and morphological aspects of pore structure are considered to describe the hysteretic behavior of SRWC.
- The calibration of the model parameters can be achieved by characterizing only both pore size and grain size distribution.

1. Introduction

The Soil Water Retention Curve (SWRC) which describes the relationship between matric suction, attributed to capillary and adsorptive forces acting between liquid, gaseous, and solid phases, and water content/degree of saturation, is known to play an important role in determining the hydro-chemo-mechanical behavior of soil. SWRC is generally determined by subjecting a soil sample to the drying, and re-wetting cycle, which consists of successive application of the increase in suction, followed by a decrease in suction.

Considering the water retention properties of the unsaturated soils, several typical observations can be deduced from the SWRC. Firstly, it is noted that the hydric path during drying is on top of the re-wetting one, which indicates a hysteresis phenomenon. Besides, there is no unique relationship between suction and water content, so the value of water content at a given suction depends on the hydric path considered. The names given to the hysteretic branches of the SWRCs are shown in Fig. 1 extracted from Pham et al. (2005). Aside from the primary curves, the initial drying curve, the boundary wetting curve, and the boundary drying curve, there is an infinite number of scanning curves inside the hysteresis loop.

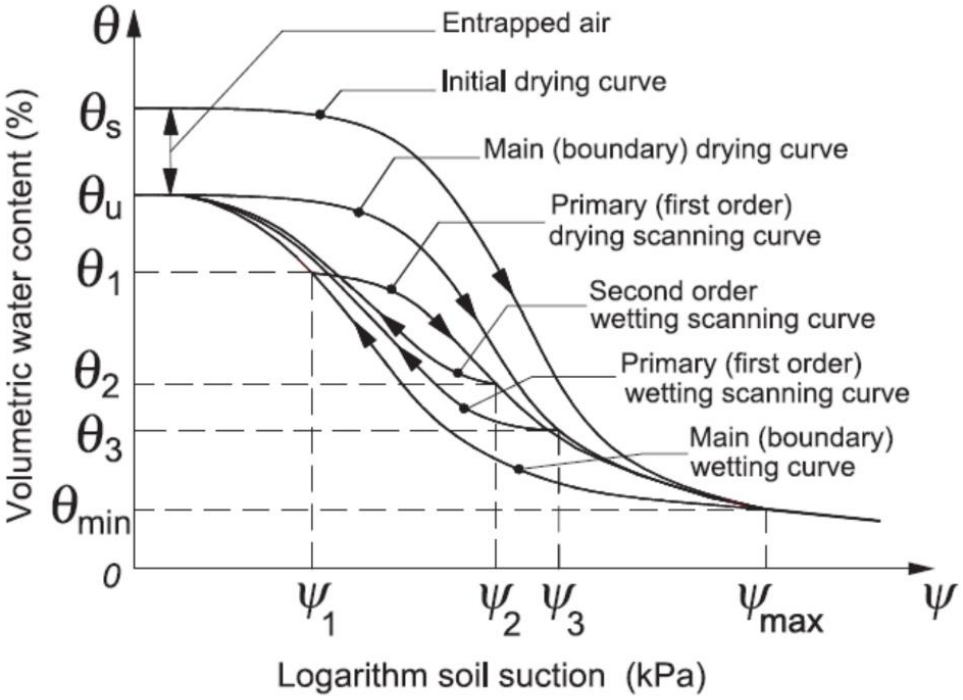

Fig. 1. Conceptual definitions used for soil-water hysteresis (from Pham et al., 2005)

The hysteresis effects in SWRC are explained by the following:

-Irregularities in the cross-sections of the void passages interconnected in series or in parallel (Delage and Cui 2000; Klausner 2012).

-Differences in contact angle during drying and re-wetting between soil particles and water (Bear 2013)

-Entrapped air, which exhibits a different volume based on the increase or decrease in soil suction.

-Thixotropic regain or aging due to the wetting and drying history of the soil.

-Difference in physical mechanisms governing drying and wetting processes: cavitation during drainage and liquid coalescence during wetting (Beckett and Augarde 2013)

Let us note that the laboratory process of determining SWRC is cumbersome, time-consuming, and expensive, as evident from studies (Carsel and Parrish 1988; Gapak et al. 2017; Haverkamp et al. 1998). For that reason, the prediction of SWRC by paying particular attention to the hysteresis effects of partially saturated soils is a challenge in the field of soil mechanics. The physical models of hysteresis can be classified into three groups: empirical models, mathematical models, and physically-based models.

As reported by Pham et al. (2005), empirical models are based on fitting the observed shape of the hysteretic SWRCs to a selected equation using empirical parameters. They can be divided into two subgroups: models that simply use the same curve fitting equation for both the wetting and drying curves but adjust the value of the parameters in each equation dependently or independently (Feng and Fredlund 1999; Karube and Kawai 2001; Kawai et al. 2000; Likos et al. 2014; Scott 1983; Tarantino 2009) and models that rely on relationships between the two boundary curves based on specified points or slopes taken at specified points (Azizi et al. 2017; Dane and Wierenga 1975; Han et al. 2019; Hayashida et al. 2003; Nimmo 1992; Wheeler et al. 2003). It is also worth noting concerning empirical models that some soils exhibit bimodal SWRC due to the presence of both macropores and micropores (dual-porosity soils). A bimodal pore size distribution is commonly observed in soils with bimodal grain size distribution (Durner 1994; Rahardjo et al. 2004; Satyanaga et al. 2013). Thus, the bimodal SWRC cannot be described using a unimodal SWRC equation (Russell 2010; Wijaya and Leong 2016). Among the numerous bimodal SWRC equations for dual-porosity soils proposed in the literature, a hysteretic model of hydraulic properties based on a fitting of modified bi-modal Van Genuchten model was proposed by Toride et al. (2013). Hysteresis is considered only in the first pore domain affecting mainly higher water contents, while a non-hysteretic behavior is assumed in the second pore domain affecting mainly lower water contents.

Different mathematical models have been proposed in the literature to predict the hysteretic behavior of water retention curves in soils (Abbasi et al. 2012; Chen et al. 2015; Pham et al. 2005). Pham

et al. (2005) have presented a list of models based on the theory of domains which consider a three-dimensional water distribution diagram involving a water function distribution. Such function explains how water in a domain can be specified as a function of two independent variables, the drying soil suction and wetting soil suction, respectively. However, most of these existing mathematical models are physically incomplete because these models only tackle the capillary hysteresis and overlook the hysteresis developed due to air-entrapment. More relevant approaches have been recently developed by Chen et al. (2015) to take both capillary and air-entrapment hysteresis into account in the SRWC model and to consider the possibility of negative matric suctions where pore water is pressurized (Chen et al. 2019). However, despite the fact that mathematical models describe well the hydraulic hysteresis of unsaturated soils, their application remains limited by the fact that measured data, *i.e.*, the boundary hysteresis loop, are required to calibrate the water function distribution. Moreover, such models do not consider and cannot predict any information about the pore structure.

Physically-based models refer to models developed based on the description of the soil pore structure associated with the water content distribution function. Hu et al. (2013) have proposed an SRWC model by considering the change in wetting and drying water retention behavior of soil based on the evolution of pore size distribution (PSD). They assumed that the PSD at a deformed state could be obtained by a vertical shifting and vertical scaling of the corresponding PSD at reference state. However, the model requires the use of several parameters.

Beckett and Augarde (2013) have also proposed a prediction of soil water retention properties with consideration of hysteresis effects by incorporating porosity and PSD combined with a more realistic arrangement of soil particles which governs the geometry of water meniscus. Larger particles have been modeled as spheres (silts and above), while clay particles have been represented as cuboids. Cavitation and liquid coalescence have been adopted by the authors as mechanisms to explain pore drainage and filling, respectively, which allows the model to predict hysteresis between drying and wetting conditions in the presence of adsorbed films without the need to consider the effects of pore interconnectivity. Nevertheless,

it is worth noting that the validation of the model was limited to the comparison with drying retention curves.

More recently, Cheng et al. (2019) have used a modeled “intrinsic” pore size distribution of soil from MIP results to predict the main drying and wetting paths of SWRC under hydro-mechanical loads. Intrinsic pore size distribution refers to the pore size distribution without the influence of pore non-uniformity encountered on MIP tests. The equations involved in the model are based on the theoretical evolutions of both pore structure (pore size distribution and void ratio) and water content distribution (as a function of pore size and matric suction) under hydro-mechanical loads. The model was validated with experimental data obtained from the literature for different types of soil despite the fact that its application was limited only to the prediction of the boundary hysteresis loop.

The present study aims to propose a new prediction model of SWRC with particular attention paid to the hysteresis phenomena encountered in partially saturated soils. As mentioned above, physically-based models allow us to achieve a more relevant physical description of moisture transport in soils. Thus, an original pore network model developed by Ranaivomanana et al. (2013, 2011) for cement-based materials is adopted for the purpose of this work. Based on experimental results of SWRC obtained on different types of soils, an adequate calibration method of parameters involved in the model is proposed and discussed in the present study regarding its transposition on soils.

2. Materials

Seven different soils obtained from literature were considered for this study. Their geotechnical properties are presented in Table 1.

Table 1:

Geotechnical properties of soil considered in the present study

Soil name	Grain Size Distribution (%)			Liquid limit (%)	Plasticity Index (%)	Specific Gravity G_s	Porosity (%)	References
	Sand (>50 µm)	Silt (2-50 µm)	Clay (< 2 µm)					
Marche Les Dames Silt	6.0	82	12	31.0	11.0	2.64	30.42	Das et al. 2020, 2021 ; Saussaye et al. 2020
Viadana Silt	2.7	76.9	20.4	32.6	8.3	2.73	39.75	Azizi et al. 2017
Pearl Clay	0	50.0	50.0	49.0	22.0	*na	na	Sun et al. 2007 cited by Han et al. 2019
Rideau Clay Loam	36.1	29.3	34.6	na	na	na	52.50	Topp 1971 cited by Han et al. 2019
Sable de Rivière				na				Vachaud 1966 cited by Assouline et al. 1998
Touchet Silt Loam				na				Jensen and Hanks 1967 cited by Assouline et al. 1998
Pachapa Loam				na				Jackson et al. 1965 cited Assouline et al. 1998

**na: not available*

3. Laboratory test

For the present study, a certain laboratory test was conducted on the compacted natural silty soil imported from Marches Les Dames (MLD), which was reported in the study of Das et al. (2020, 2021) for the validation of the model.

The water content and suction measurements of the natural MLD silty soil were conducted by oven drying at 105˚C (ASTM 2010) and by using WP4C Dewpoint Potentiometer (Decagon device), respectively.

For microstructural analysis, compacted specimens were freeze-dried and then subjected to Mercury Intrusion Porosimetry (MIP) and Brunauer-Emmett-Teller (BET) tests. During the MIP test, freeze-dried specimens of $1cm^3$ were placed inside a sealed penetrometer and then evacuated via heating under vacuum or flushing with an inert gas (Espinal 2002). After evacuation, mercury was progressively introduced into the samples through incremental hydraulic pressure steps. The volume of mercury intruded, V (ml/g), and the applied pressure, p (MPa), is recorded (Klobes and Munro 2006). By measuring the pressure required to be applied to force the mercury into a cylindrical pore diameter were obtained using the Washburn equation.

BET is a nitrogen gas adsorption technique for measuring the Specific Surface Area (SSA) of the soil (Brunauer et al. 1938). Freeze-dried samples were evacuated or degassed to remove moisture, vapor, and any other unwanted gas species from the pore surface at 50°C. Nitrogen gas at 77K and at a pressure lower than the equilibrium/saturation gas pressure (p_0) is then injected, and the first forms monolayer adsorption of nitrogen molecules give the value for SSA. Further increasing the gas pressure cause formation of multilayer adsorption over the monolayer. Once the saturation pressure (p_0) is reached, the completion of the adsorption phase occurs, and the desorption phase is initiated, in which the gas is progressively withdrawn until the initial point of the adsorption phase is achieved. These adsorption and

desorption branches characterize the PSD inside the soil mass. This procedure of obtaining the PSD is regarded as Barrett-Joiner-Halendapore (BJH) (Barrett et al. 1951).

4. Description of the model developed by Ranaivomanana et al. (2011, 2013) to predict water vapor sorption/desorption isotherms on cement-based materials

4.1. Principles of the model

The model developed by Ranaivomanana et al. (2011, 2013) for cement-based materials consists of an idealized PSD of a unit volume of material with 3 modes associated with C-S-H pores and with narrow and wide capillary pores, respectively. Firstly, it is worth specifying that the liquid phase considered in the present study is an inert wetting-fluid. The wide capillary pores are assumed to play an essential role in the water permeability of the saturated material since their drainage has an impact on the continuity of the percolated part of the liquid phase. Moreover, the latter would form a path connected to the surface of the material which is responsible for the sharp drop of desorption isotherms observed experimentally at high relative humidity (RH). In the pore size classification proposed by Mindess et al. (2002) and adopted for the pore network model, the C-S-H gel pores are smaller than 0.010 µm. Thin capillaries are between 0.0025 µm and 0.050 µm, and large capillaries are between 0.050 and 10 µm.

4.2. Pore size distribution, pore connectivity, and management of hysteresis

A porous mode is represented by four portions of parabolas, each of which is set to a range of log (r) equal to the amplitude δ and height on the axis dV/dlog (r) equal to ξ as seen in Figure 2. Each of the three modes is characterized by three parameters: the radius of the central mode r_{mode}, the amplitude δ, and the height ξ.

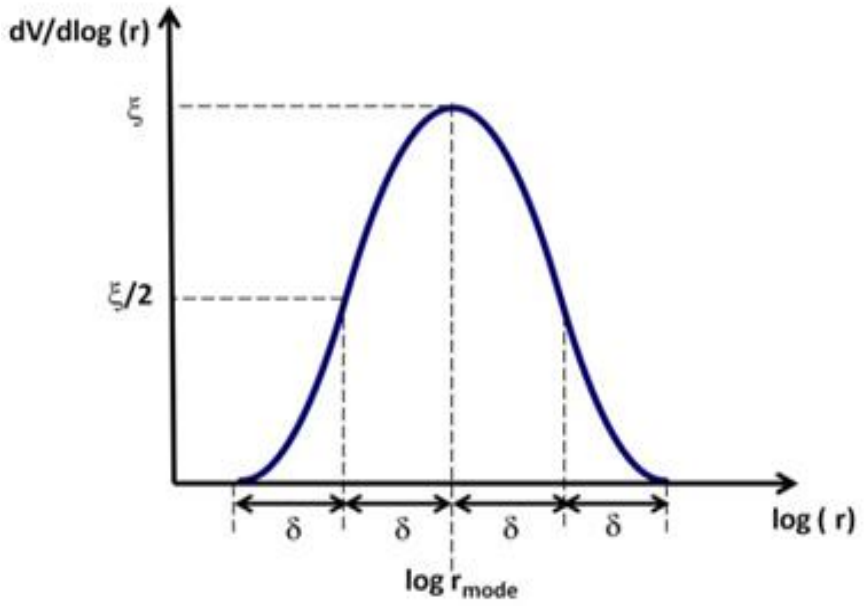

Fig. 2. Representation of one porous mode with four portions of parabola

For a distribution containing 3 modes, we have:

$$\frac{dV}{d\log r} = \bigcup_{i=1}^{i=3}\left(\bigcup_{j=1}^{j=4}\left(\beta_{ji}^{1}(\log r)^2 + \beta_{ji}^{2}(\log r) + \beta_{ji}^{3}\right)\right) \quad (1)$$

where the coefficients β_{ji}^{k} (k=1 to 3) depend on r_{mode}, δ and ξ.

Referring to the classification proposed by Mindess et al. (2002), the following values were imposed: δ = 0.4 associated with a value of r_{mode} fixed at 0.0015µm for the first mode ($r_{C\text{-}S\text{-}H}$) and 0.0095 µm for the second mode (r_{narrow}). A constant value of 0.3 µm was assigned to r_{wide} according to different classifications of large capillaries range proposed in the literature. The height of each mode is assumed to be proportional to its porosity. The 1st mode, corresponding to C-S-H pores, is calibrated by calculating the volume of C-S-H formed per unit volume of material by using a cement hydration model. The acronym C-

S-H means Calcium Silicate Hydrate. It is the main product of the hydration of Portland Cement and is primarily responsible for the strength in cement- based materials. The volume of the 3rd mode, associated with wide capillaries, r_{wide}, was directly deduced from the sharp drop of the desorption isotherm at high RH. It means that the prediction of water sorption/desorption curves from the model requires at least the experimental achievement of moisture equilibrium at high RH.

In most of the pore network models developed earlier for the prediction of transport properties of cement-based materials, pores are generally represented with cylindrical geometry. However, a flattened morphology seems more conceivable for small pores. This seems to corroborate the representation of C-S-H with a layered structure. For this purpose, Ranaivomanana et al. (2011, 2013) have proposed an oblong geometry for pores with lower radii.

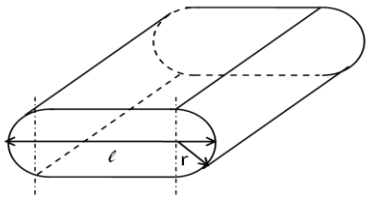

Fig. 3. Oblong shaped pore (after Ranaivomanana et al. (2011, 2013))

The oblong shape (Fig. 3) can be characterized by an aspect ratio A_p defined as the ratio between the width and the height of the pore cross-section. For the reasons mentioned above, the coefficient A_p evolves to flatten the pores with a small radius. For this purpose, an exponential equation given by Eq. 2 was used:

$$A_p = \frac{l}{2r} = max\left[exp\left(\frac{r_{cr}}{r}; 1\right)\right] \qquad (2)$$

where r_{cr} is a calibration parameter called the "critical radius". This parameter may be interpreted as the pore radius below which pores are more oblong shaped compared to cylindrical shape. Indeed, according to equation 2, the large pores are cylindrical, as their aspect ratio slightly exceeds 1 and the pores become progressively flattened as r decreases. By an inverse analysis conducted on different types of cementitious materials, Ranaivomanana et al. (2013) have suggested a value of 0.002 µm for r_{cr}.

The pore cross-sectional area, a(r) is given by the relationship:

$$a(r) = \left[4\left(A_p(r) - 1\right) + \pi\right]r^2 \qquad (3)$$

In order to model the isotherms, while paying particular attention to the hysteresis effect, it was assumed that the drying of a pore is possible only if it is connected to the dry fraction of the pore network. The hysteresis between desorption and adsorption isotherms is the consequence of the presence of "ink bottle" shaped pores. This leads to the drying of a greater part of the pore volume at low RH. We can therefore consider that drier is the material, higher is the probability of the connection of a saturated pore to the dry fraction of the pore network. This seems to provide a logical explanation for the decrease of hysteresis in the area of low RH. Assuming that drying affects pores with size r_i when the relative humidity is h_i, the drained portion of the porous network represents a fraction of pores of radius larger than r_1. This fraction depends on the connectivity between the drained portion and pores of radius r_1. It is very likely that longer the developed length of pores with radius bigger than r_1, greater is their potential connectivity. In fact, most of these pores are long, so they are able to interconnect pores of various sizes. For this reason, it was assumed that the probability of interconnection $P_{int}(r > r_i)$ of pores with a radius greater than r_i can be approximated by the ratio between the total length of pores for which $r > r_i$ to the cumulative total length of all pores of the network considered.

$$P_{int}(r > r_i) = \frac{\int_{r_i}^{r_{max}} \frac{1}{a(r)} \frac{dV}{dlogr} dlogr}{\int_{r_{min}}^{r_{max}} \frac{1}{a(r)} \frac{dV}{dlogr} dlogr} \quad (4)$$

where $a(r)$ is the pore sectional area defined by Eq. 4. $dV/dlogr$ is the density function of the PSD, approximated by Eq. 1 in the model.

The probability of connection P_{int} concerns the C-S-H pores and the narrow capillaries only because the connectivity of wide capillary pores was assumed to be maximal (P_{int}=1) as they are supposed to form a path connected to the surface of the material. So, the function P_{int} was normalized by Ranaivomanana et al. (2011) with respect to the porosity corresponding to each mode.

If the RH decreases from h_i *to* $h_j < h_i$, then the pores with radii between r_i and r_j (corresponding to h_j) are partially drained. The residual saturation degree of pores with radii greater than r_j, noted S_{ink} is in the context of the present model, dependent on their connectivity to the dry fraction of the network. As a first approximation, the following relationship (Eq. 5) was adopted:

$$S_{ink} = 1 - P_{int}^{*}(r > r_j) \quad (5)$$

If the RH increases from h_i to h_k, pores with sizes between r_i and r_k (corresponding to h_k), which belong to the dry portion of the network, are instantly saturated again. Of course, the volume of water in pores with radii greater than r_k, which can be drained only via smaller pores remains constant. The mechanisms of the evolution of the degree of saturation of a pore with a given radius are detailed in the study of Ranaivomanana et al. (2011).

Given that the management of saturation increments based on relative humidity increments is easy only on a numerically discretized porous network, the PSD was discretized, and the probability of interconnection (Eq. 4) was approximated by linear interpolation from one discrete radius to another. A

sensitive analysis of the model parameters conducted by Ranaivomanana (2010) has shown that beyond a value of 100 (for the entire PSD), the number of discretization has no effect on the simulation results.

Finally, let us remind that water retention curves are expressed in terms of matric suction for soils rather than in terms of RH. Nevertheless, a relationship given by Kelvin's law (Eq. 6) exists between the two quantities.

$$\psi = -\rho_l \frac{RT}{M_v} \ln h \quad (6)$$

where:

- ψ, the matric suction (Pa),
- h, the relative humidity
- T, the temperature taken equal to 293 K (20°C)
- ρ_l, the density of water taken equal to 1000 kg/m^3
- R: the perfect gas constant (8.32 J/K/mol)
- M_v: the molar mass of water (18 x 10^{-3} kg/mol)

5. Application of the model developed by Ranaivomanana et al. (2011, 2013) to the prediction of SRWC

5.1. Modeling strategy

The model developed by Ranaivomanana et al. (2011, 2013) would seem to be well-adapted to the prediction of SRWC of soils. Indeed, PSD allows to take into account explicitly the double porosity aspect associated with macropores (mostly the inter-aggregate pores between aggregations) and micropores (intra-

aggregate pores) respectively and can be involved in the implementation of physically-based models (*e.g.*, Beckett and Augarde 2013; Casini et al, 2012; Cheng et al. 2019; Hu et al. 2013; Prapaharan et al. 1985; Romero et al. 1999; Simms and Yanful 2002, 2001). However, according to Cheng et al. (2019), the PSD obtained from MIP is affected by the pore non-uniformity and does not represent the intrinsic PSD of soil. Thus, a relevant description of the realistic PSD of soils could be achieved by the model proposed by Ranaivomanana et al. (2011). Moreover, the representation of C-S-H pores with an oblong geometry could also be adjusted to soils given that the crystalline structure of clay minerals is built up from different types of sheets or layers. A similar approach was adopted previously by Beckett and Augarde (2013) or by Barast et al. (2017) with a representation of clay particles as cuboids.

However, given that soil structure or fabric mainly depends on its composition and texture and is also strongly affected by the application of chemo-hydro-mechanical loadings (*e.g.*, Al-Mukhtar et al. 1996; Coulon and Bruand 1989; Cuisinier and Laloui 2004; Delage and Lefebvre 1984; Griffiths and Joshi 1989; Ranaivomanana et al. 2018, 2017; Simms and Yanful 2001), the pore structure of soils cannot be described with a unique set of parameters values as adopted by Ranaivomanana et al. (2011) for cement-based materials. Thus, for the purpose of applying the model developed by Ranaivomanana et al. (2011) to soils, the strategy adopted in the present study consists first in calibrating the model parameters from an inverse analysis of SWRC. Once the values of the parameters are calibrated, they are discussed and compared with measured data from the literature in order to propose a relevant calibration method that can be directly deduced from soil fabric.

Let us recall that the model proposed in the present work is mainly based on the interconnection of pores and does not consider other possible factors which may also explain the hysteretic behavior of SWRC. For that reason and given that the contact angle values of soils considered in this study are not available, a simplifying assumption of constant contact angle during both drying and wetting phases is adopted. Moreover, the role of the contact angle in SWRC has not been adequately recognized. Different modeling approaches describing the evolution of contact angle with pore size have been proposed in the literature. However, analytical approaches may involve many fitting parameters (Liu et al. (2013)) while both

multiphysic and multiscale approach require a description of particles shape combined with a realistic representation of their arrangement (Beckett and Augarde (2013)). Another important aspect that has to be considered in the modeling of SWRC is the volume change that may occur as a result of changes in the moisture content more particularly on clay rich soils (shrink-swell behavior). However, these volume changes are neglected in the present study due the variety of soils tested. On the other hand, they have not been considered in the original version of the model developed for cement-based materials which may also exhibit a volume change behavior. Nevertheless, the recent findings on those aspects (Sun and Cui, 2020, Zhai et al., 2020) could be used in a further development of the model.

A schematic diagram describing the drainage of the pore network as function of suction values is represented in Figure 4.

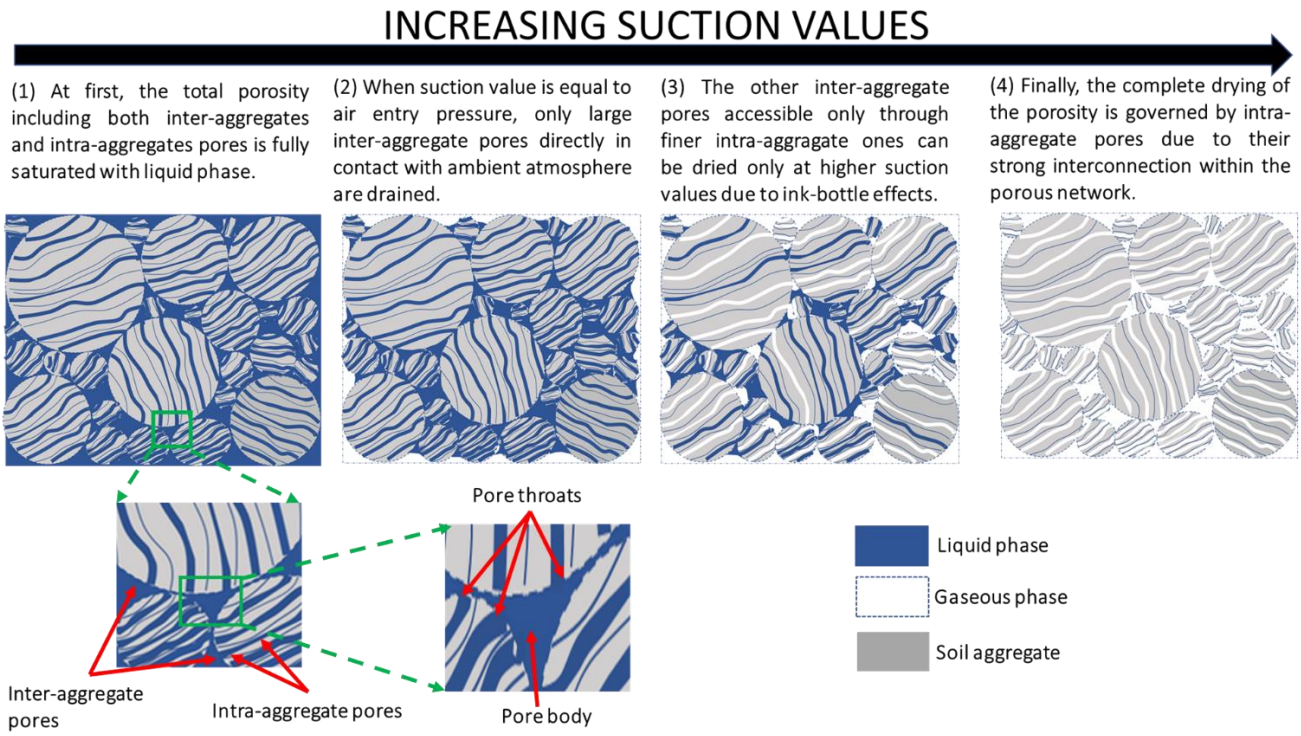

Fig. 4. Schematic diagram describing the drainage of the pore network as function of suction values

334 *5.2. Results and discussion*

335

336 *5.2.1. SWRC with hysteresis effects*

337 Firstly, the only available drying paths that have been experimentally measured for soils named
338 "Sable de Rivière", "Pachapa loam" and "Touchet silt loam" respectively (soils cited and studied by
339 Assouline et al. 1998) are compared with the simulated drying paths to illustrate the ability of the model to
340 predict only the drying path (Figs. 5 to 7). Despite the fact that experimental wetting paths are not available
341 (probably not measured) for the previous soils, the corresponding simulated wetting paths are also
342 represented in order to confirm the potentiality of using the model to predict hysteretic effects.

343

344

345

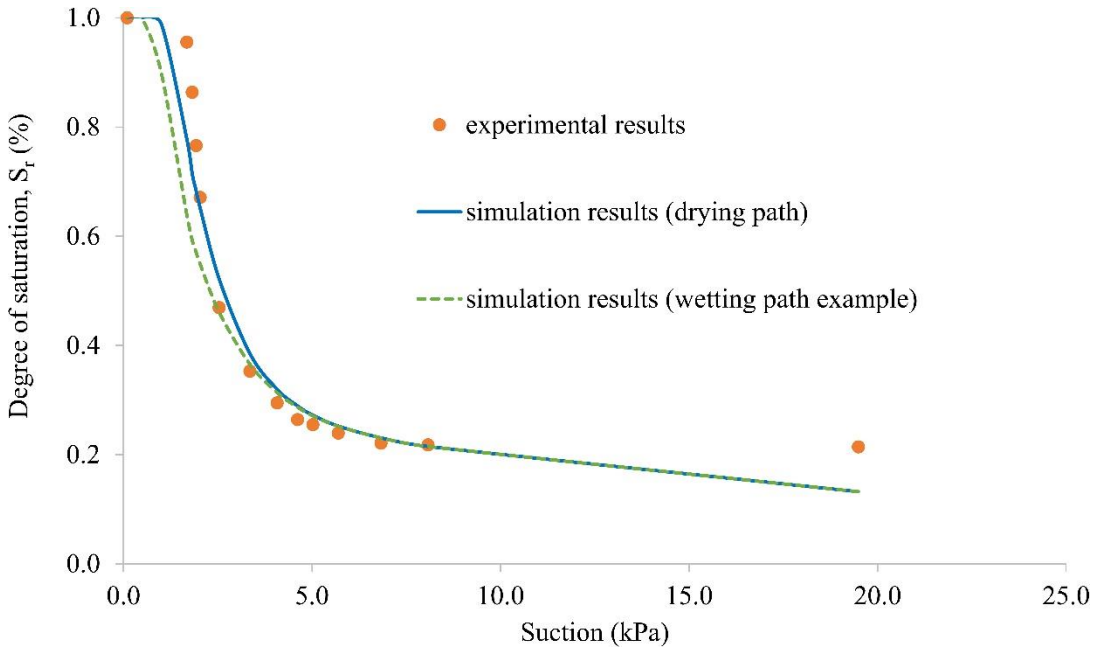

346

347 **Fig. 5** Experimental results and simulated results of SWRC on Sable de Rivière (Vachaud 1966 cited by Assouline et al. 1998)

348

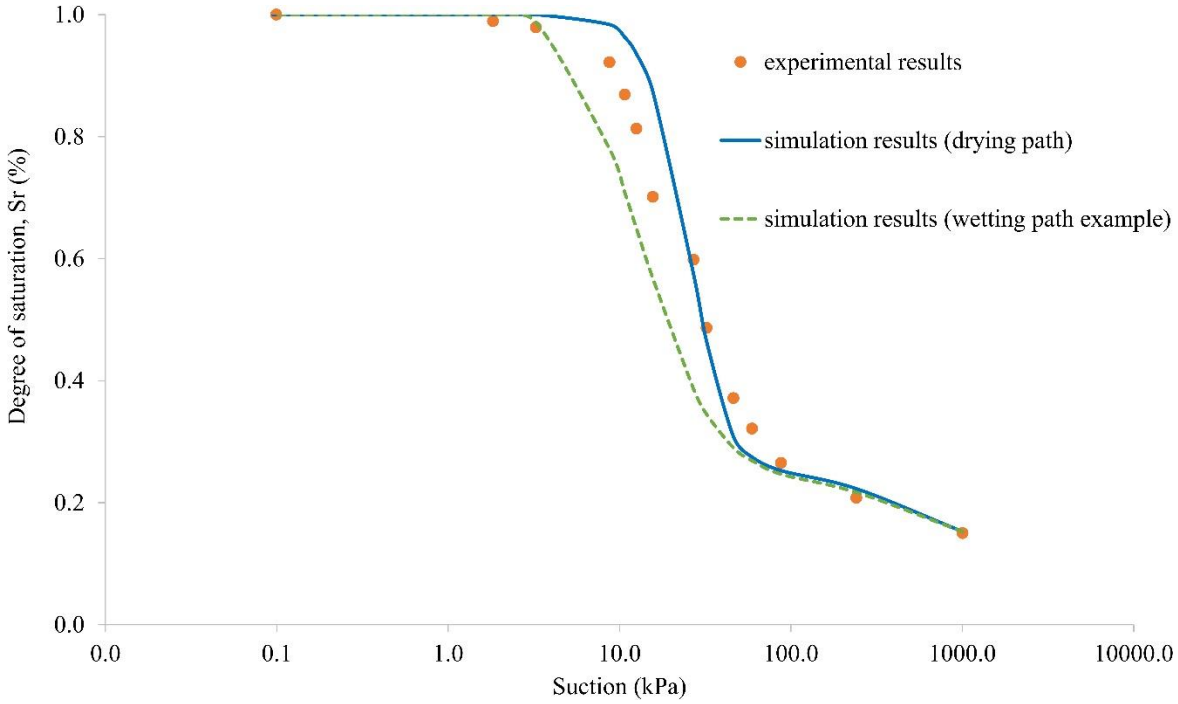

Fig. 6. Experimental results and simulated results of SWRC on Pachapa Loam (Jackson et al. 1965 cited Assouline et al. 1998)

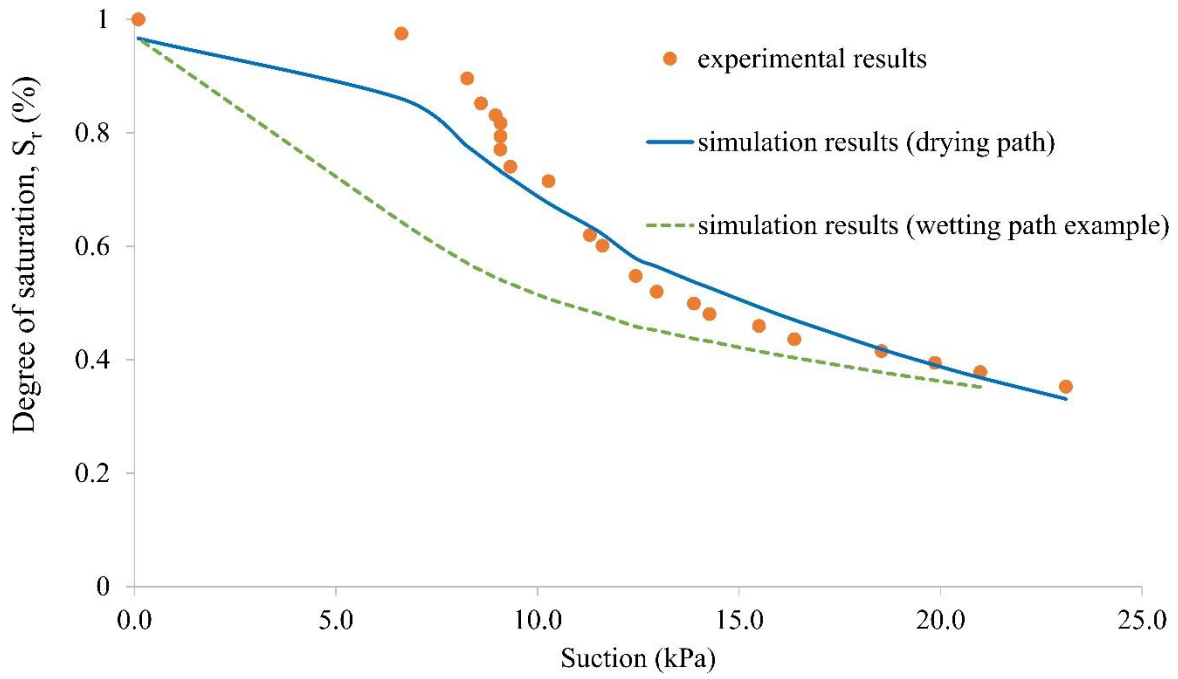

Fig. 7. Experimental results and simulated results of SWRC on Touchet Silt Loam (Jensen and Hanks 1967 cited by Assouline et al. 1998)

Secondly, both available drying and wetting paths that have been experimentally measured for soils named “Pearl Clay”, “Viadana Silt” and “Rideau Clay loam” respectively (soils cited by Azizi et al. 2017 Han et al. 2019) are compared with the simulated drying and wetting paths from Figs. 8 to 10. Yet again a satisfiable stimulated wetting and drying curves were generated showing the accuracy of the model in predicting a complete SWRC curves.

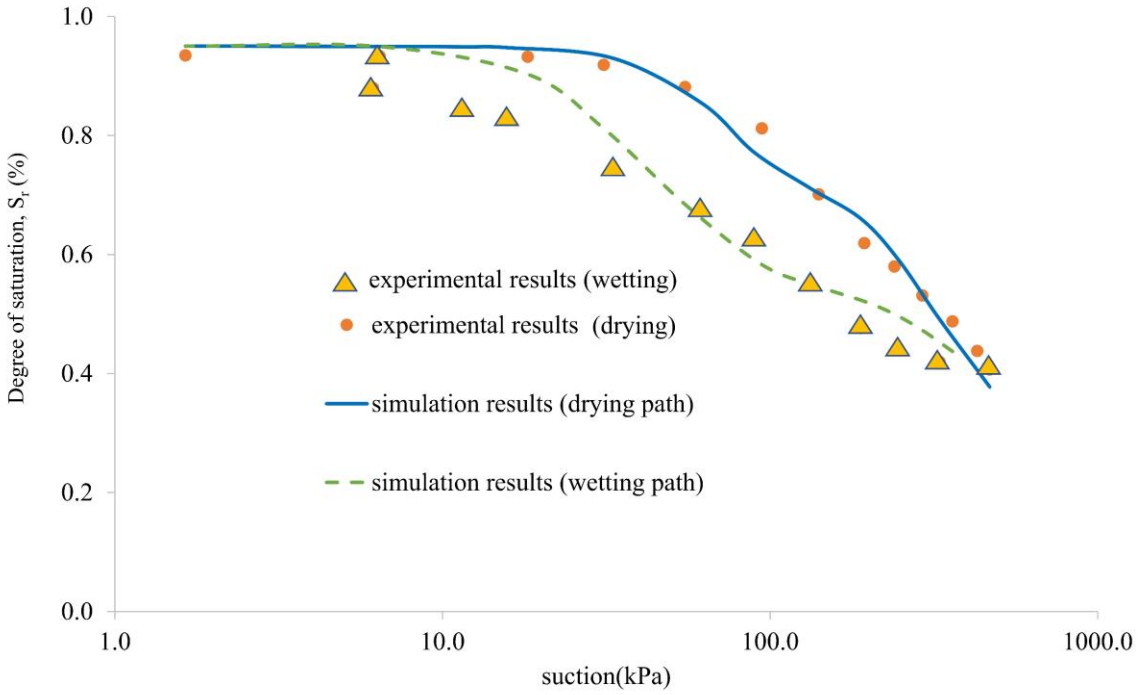

Fig. 8. Experimental results and simulated results of SWRC on Pearl Clay (Sun et al. 2007 cited by Han et al. 2019)

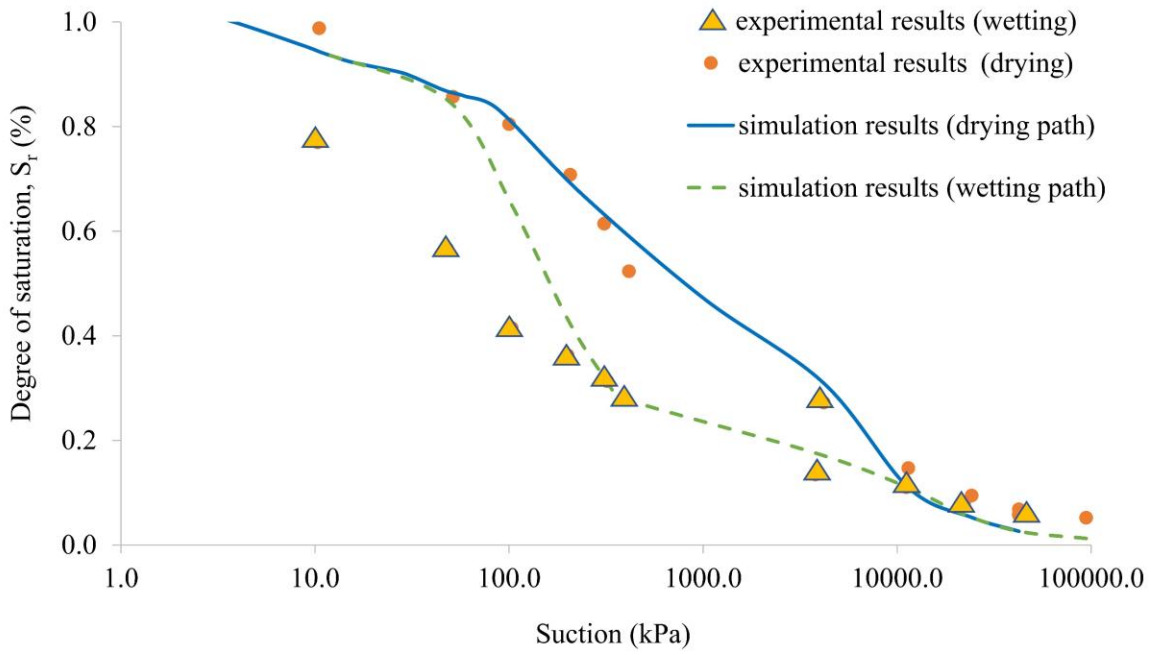

365

366 **Fig. 9.** Experimental results and simulated results of SWRC on Viadana Silt (Azizi et al. 2017)

367

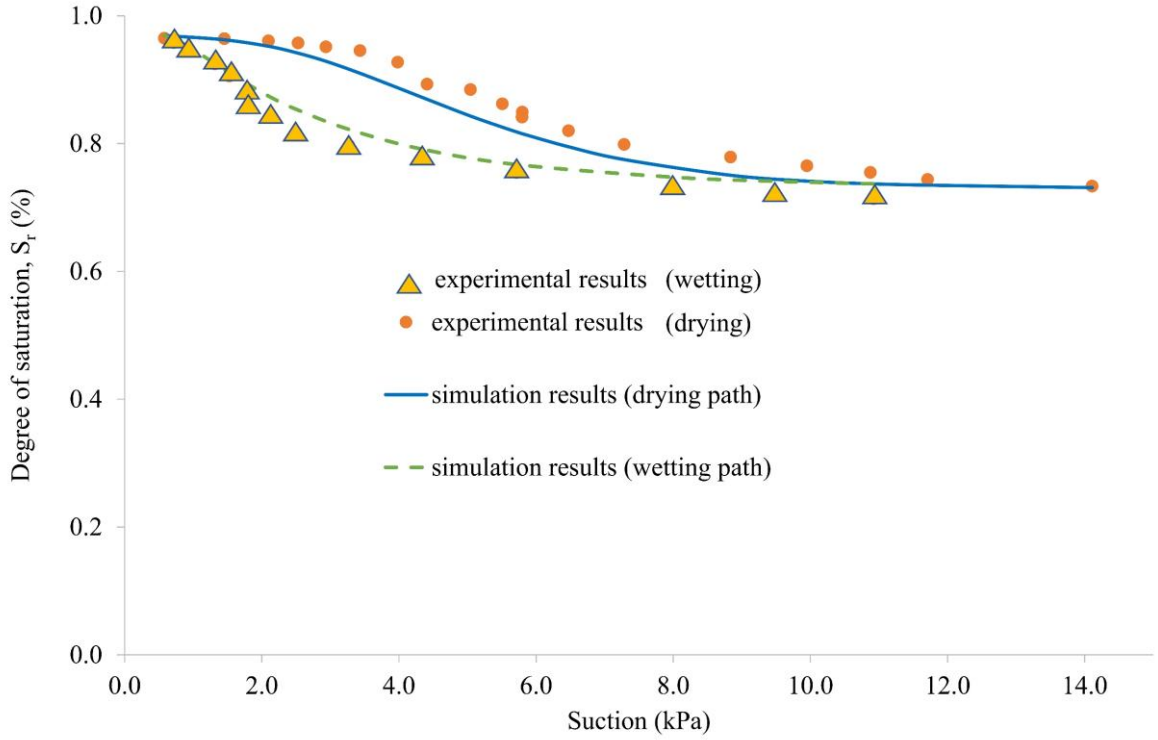

368

369 **Fig. 10.** Experimental results and simulated results of SWRC on Rideau Clay loam (Topp 1971 cited by Han et al. 2019)

370

Given that only available drying paths and both wetting and drying paths hysteresis obtained from the literature were comparable with the one predicted by the model, the present model attempt to validate its accuracy with reduced number of experimental points in Fig. 11. Fig. 11 validates the applicability of the model in MLD soil with only two points, *i.e.*, an experimental wetting and drying suction values.

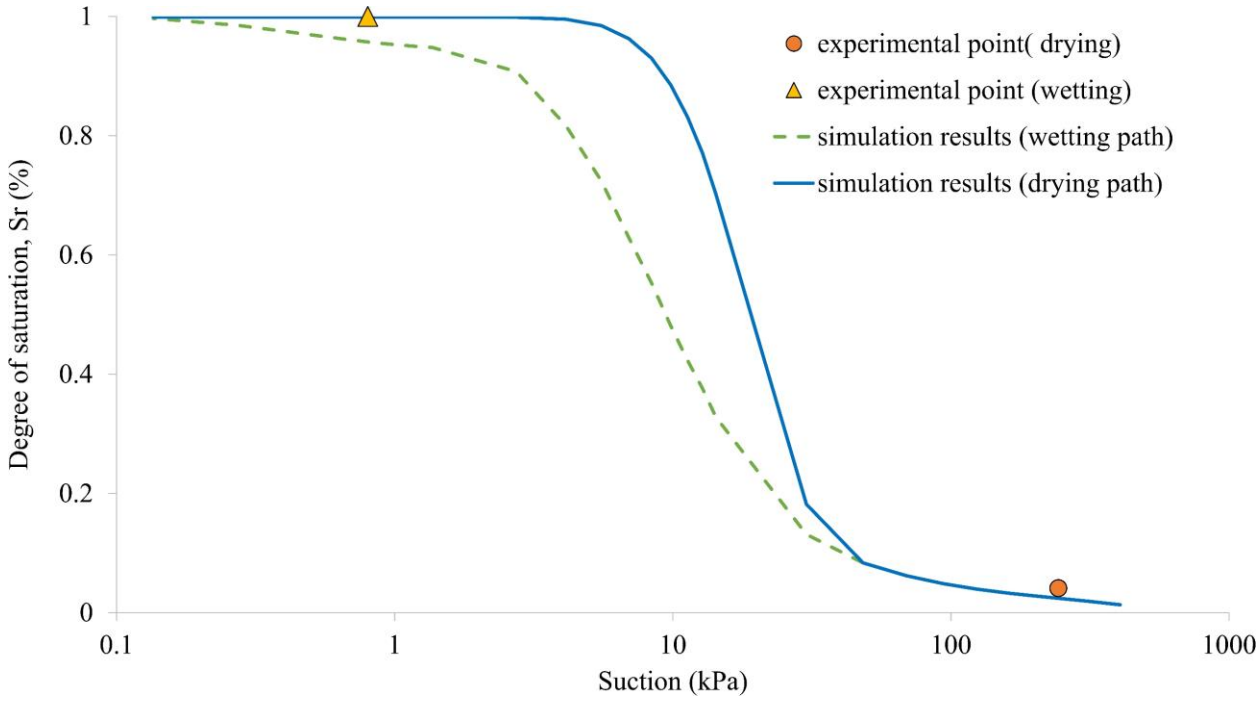

Fig. 11. Experimental results and simulated results of SWRC on Marche Les Dames Silt

The model parameters values deduced from an inverse analysis of SRWC are presented in Table 2. The corresponding idealized PSDs are presented in Figs 12 to 18.

Table 2:

Values of the parameters involved in the model for soils considered in the present study

Soil name	1st porous mode		2nd porous mode		3rd porous mode		δ	r_{cr} (µm)
	$r_{mode,1}$ (µm)	% porosity	$r_{mode,2}$ (µm)	% porosity	$r_{mode,3}$ (µm)	% porosity		

Marche Les Dames Silt	0.025	94	0.5	6				0.002
Sable de Rivière	5	15	80	85				150
Touchet silt loam	5	40	35	60				21
Pachapa loam	0.085	20	15	80			0.4	2.5
Pearl clay	0.19	48	5	47	3000	5		1.6
Viadana Silt	0.01	17	1.7	68	30	15		0.12
Rideau clay loam	0.25	65	90	32	3000	3		7

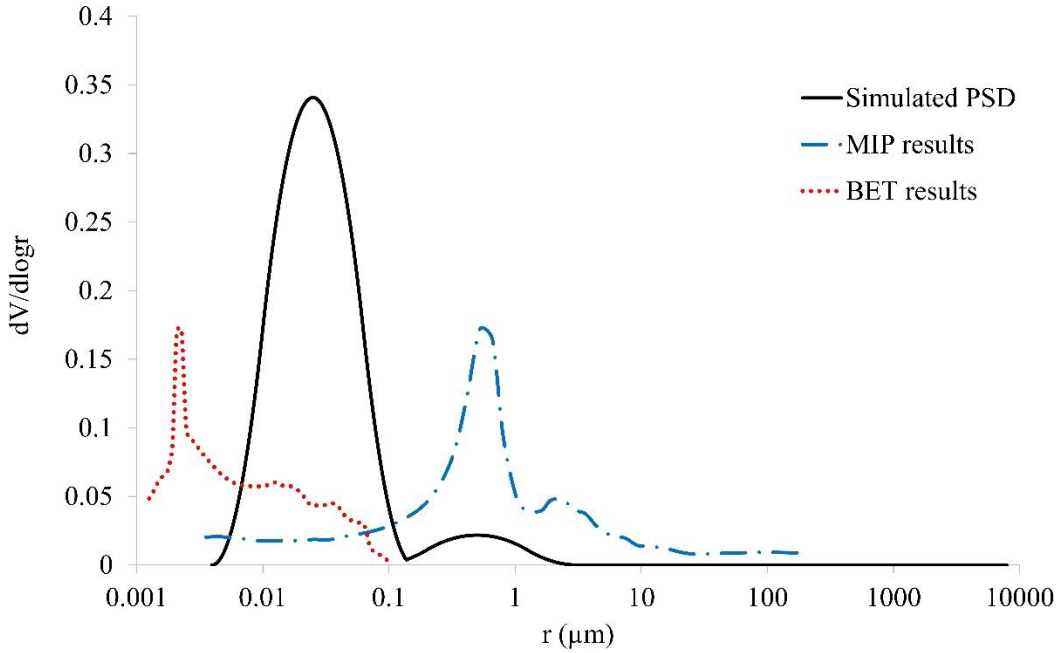

Fig. 12. Experimental and simulated pore size distribution of Marche Les Dame Silt

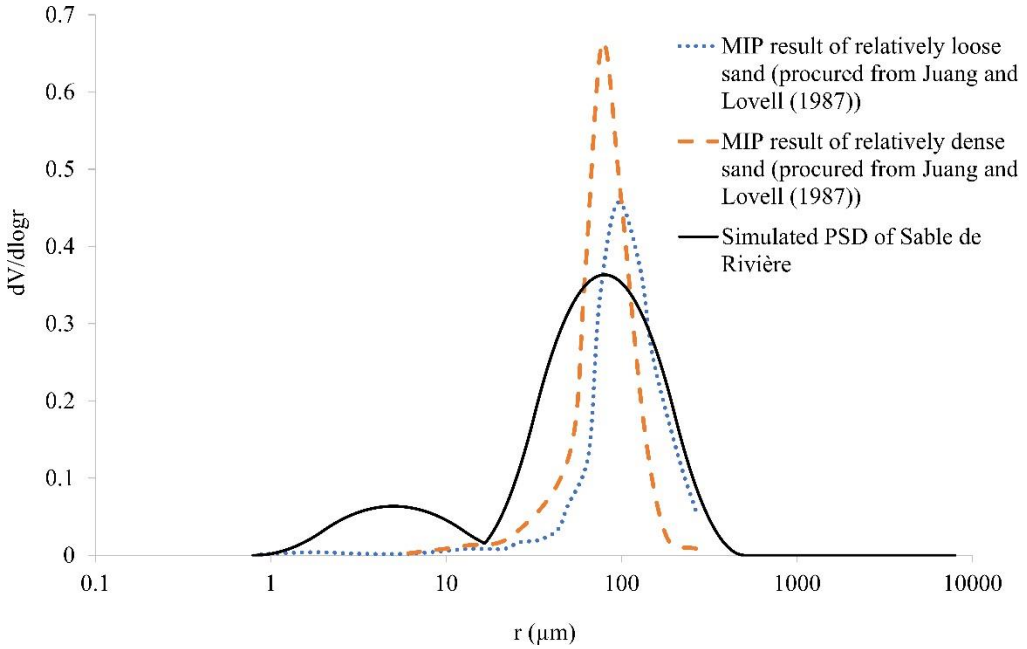

392

393 **Fig. 13.** Experimental and simulated pore size distribution of Sable de Rivière

394

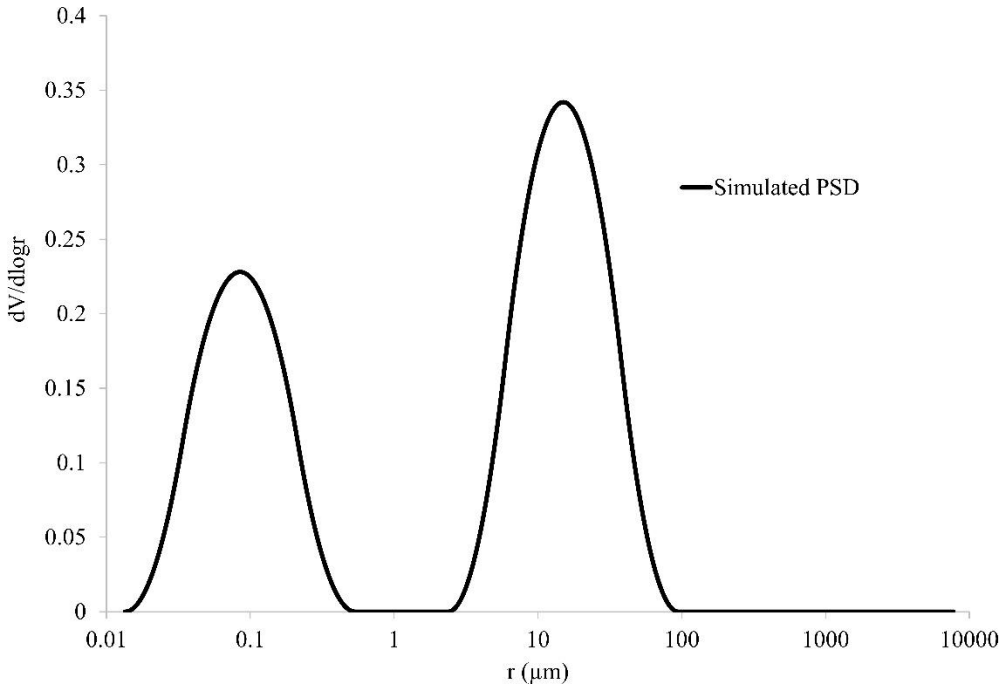

395

396 **Fig. 14.** Simulated pore size distribution of Pachapa Loam

397

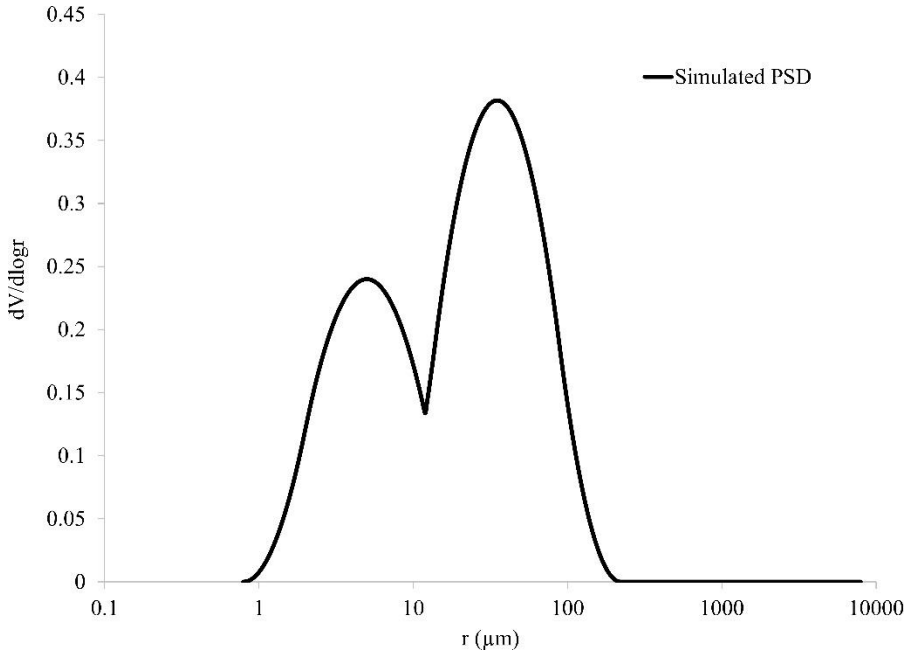

398

399 **Fig. 15.** Simulated pore size distribution of Touchet Silt Loam

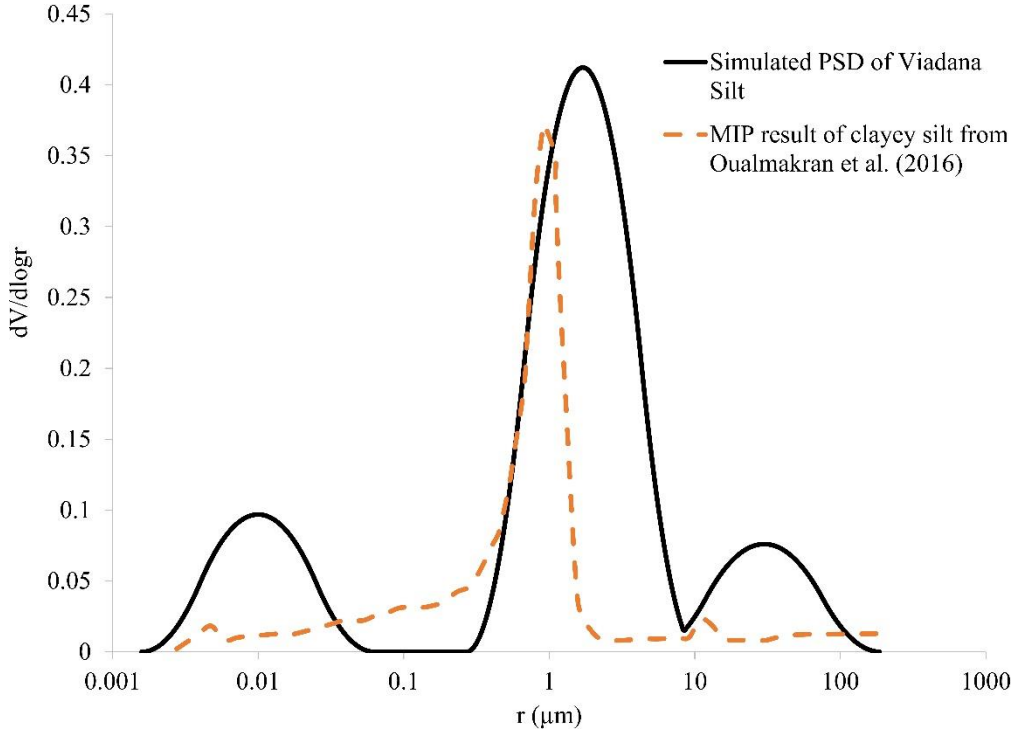

400

401 **Fig. 16.** MIP result of a clayey silt and simulated pore size distribution of Viadana Silt

402

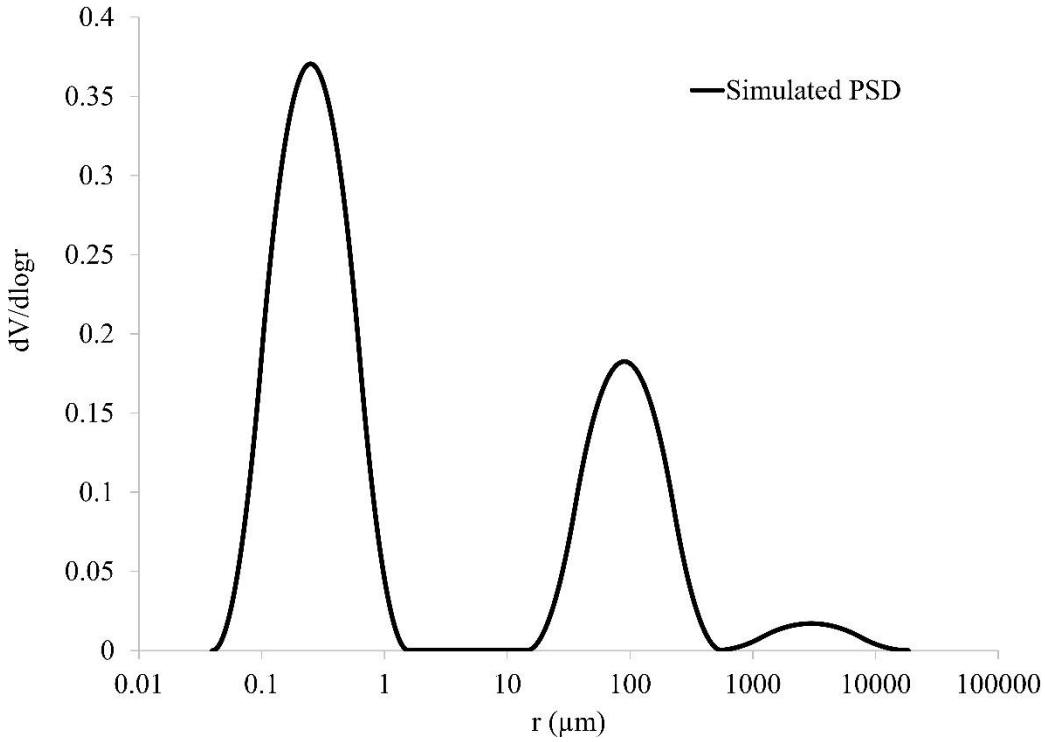

403

404 **Fig. 17.** Simulated pore size distribution of Pearl Clay

405

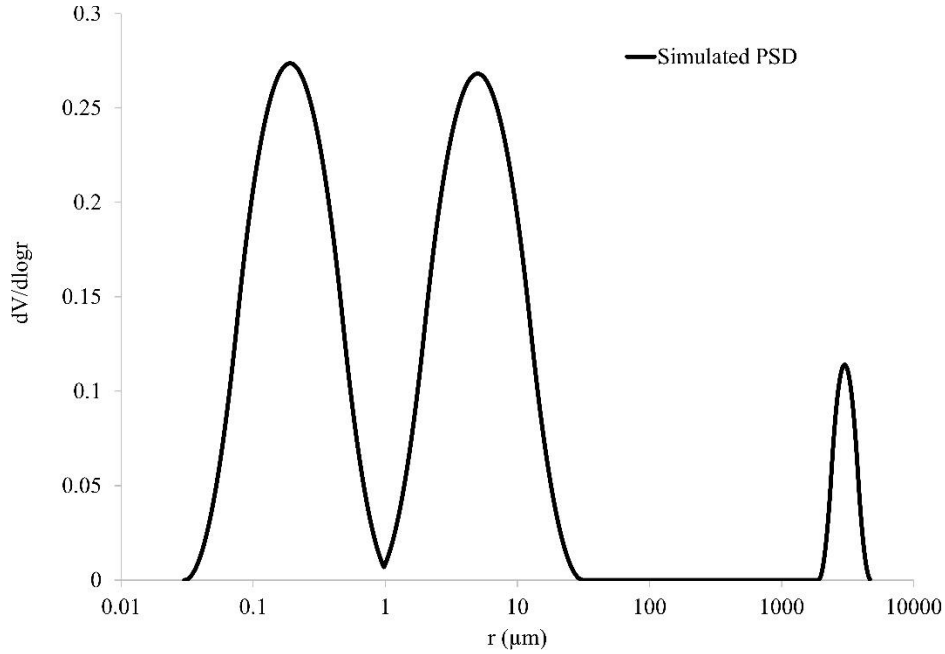

406

407 **Fig. 18.** Simulated pore size distribution of Rideau Clay Loam

408

409

5.2.2 Calibration of porous mode values r_{mode}

Except for Pearl clay, Viadana Silt, and Rideau clay loam, soils considered in the present study exhibit two porous modes (Figs. 12 to 18). The first mode, located between 0.5 and 80µm, is probably associated with interaggregate macropores, while the second one located between 0.025 and 5µm, probably corresponds to intra-aggregates micropores. According to the values shown in Table 2, it can be observed that the value of macropore mode tends to decrease with the increase of the percentage of fine elements. Such results are consistent with those obtained by Ranaivomanana et al. (2017). For sandy soil named "Sable de Rivière," a mode value of 80µm was found (Fig. 13). For loamy soils named "Touchet Silt loam" and "Pachapa loam".which were composed of silt, clay, and sand, a lower mode value was obtained (35 and 15µm, respectively) (Figs. 14 & 15). Finally, for silty soil named "Marche Les Dame Silt", which contains the lowest percentage of sand (6%), a mode value of 0.5µm was found (Fig. 12). Concerning the loamy soil named "Rideau clay loam", the two porous modes located at 90 and 3000µm respectively correspond to macropores, including probable microcracks, while the first mode located at 0.25µm belongs certainly to intra-aggregates micropores (Fig. 18). Similarly, for the clayey soil named "Pearl clay", which is a fine soil, the porous mode observed at 3000µm can also be interpreted as the result of microcracking. The two other modes observed at 0.19 and 5 µm, respectively, can be considered as being part of clay micropores (Fig. 17).

Comparatively to loamy soils, the presence of a low percentage of sand (2.7%) in the silty soil named "Viadana Silt" probably explains the formation of the macropores porous mode identified at 30µm (Fig. 16). The two other mode's values located at 0.01 and 1.7µm, respectively, are associated with micropores.

The evolution of micropores mode value seems to be more dependent on the amount and the mineralogy of clays which vary from one soil to another than on particle size distribution and presence of microcracks, in comparison with macropores mode value.

The results mentioned above, thus, confirmed the heterogeneity of the pore structure of soils as already mentioned in section 5.1 and the difficulty to achieve a description of the idealized PSD with a

436 unique set of parameter values as adopted by Ranaivomanana et al. (2011) for cementitious materials. For
437 that purpose, the use of MIP appears as an adapted tool to calibrate the values of porous modes of
438 macropores and micropores, respectively. The relevance of such calibration method is validated by the
439 similarities between the porous mode values deduced from simulations and those obtained from MIP results
440 which have been measured experimentally for silty soil named "Marche Les Dames Silt" (Fig. 12) and
441 extracted from literature for sandy soil named "Sable de Rivière" (Fig. 13) and for silty soil named "Viadana
442 Silt" (Fig. 16), respectively (Juang and Lovell 1986; Oualmakran et al. 2016).

443 Finally, it can be observed in Fig. 12 that the PSD of silty soil named "Marche Les Dames Silt",
444 obtained from BET measurements reveals the presence of a porous mode associated with micropores
445 located around 0.002µm. Such porous mode, which has already been detected in previous studies (for
446 example, Kuila and Prasad 2013), was not considered in the characterization of the dual structure of soils
447 porosity (Casini et al. 2012; de la Morena et al. 2021; Li and Zhang 2009). In fact, water flow is considerably
448 slow in smaller pores (Committee and America 2008; Sumner 1999), and its removal is possible only when
449 the soil is significantly dry. Nevertheless, the SSA of soils is mainly attributed to the presence of those
450 small pores, and the SSA obtained from BET measurements being generally much higher than that provided
451 by MIP results. Besides, the model proposed in the present study can provide the SSA values of the soil
452 particles by multiplying pore perimeters by their developed lengths as performed in Ranaivomanana et al.
453 (2011). For silty soil named "Marche Les Dames Silt", an SSA of 14m²/g was obtained by considering only
454 the porous modes obtained from MIP test while a higher value equivalent to that provided by the BET
455 method, *i.e.*, 21 m^2/g, was found when the porous mode associated with small pores (detected only with
456 BET measurements and not with MIP tests) was considered. The results obtained confirmed and validated
457 the role played by small pores in the estimation of the specific surface area, even if their contribution to
458 water movement is often neglected.

459

460

461 *5.2.3 Calibration of the amplitude δ of a porous mode*

462 Ranaivomanana et al. (2011) obtained an amplitude, δ equal to 0.4 (in log(r), where r is in nm), for
463 cement –based materials. In the present case, despite the fact that the porous structure of cementitious
464 materials and that of soils are not comparable in terms of mode values, the amplitude of the latter is
465 approximately of the same order of magnitude as seen in Table 2.

466

467 *5.2.4 Calibration of the height ξ of a porous mode*

468 As already specified in section 4.2, the height ξ of a porous mode was assumed to be proportional
469 to its porosity. For cement-based materials, the partition of the porosity between large capillary pores and
470 small C-S-H pores can be estimated using hydration models (Ranaivomanana et al. 2011). For soils, it may
471 be considered that the volume of micropores depend on the fine fraction, particularly on the clay fraction.
472 Given that different clay structures can be encountered in soils, mineralogical aspects should also be
473 considered in order to estimate the porosity related to micropores more precisely. However, these aspects
474 will not be addressed in the present study.

475 As a first approximation, it was decided to correlate the volume of macropores with the coarse
476 fraction of soils, which affects the mode value of macropores, as seen previously. Indeed, it can be assumed
477 at the granular level that the higher is the fine fraction, the lower is the macropore porosity. Such assumption
478 can be physically justified by the fact that the porous spaces between coarse elements corresponding to
479 macropores are filled with finer particles resulting in a decrease in macropores porosity. For soils
480 considered in the present study, it can be observed in Fig. 18 that the porosity fraction associated with
481 macropores was almost equivalent to the sand fraction, thereby corroborating the existence of a correlation
482 between the two quantities as mentioned above. For clayey soil named “Pearl clay”, which is composed
483 only of silt and clay (see Table 1), a porosity fraction corresponding to macropores equal to 5% was found.
484 Such value gap can be attributed to the presence of microcracking, which also probably explains the results
485 obtained for silty soil named “Viadana Silt” (see section 5.2.2.1). Let us notice that the sandy soil named

"Sable de Rivière" and loamy soils named "Touchet Silt loam" and "Pachapa loam" respectively are not represented in Fig. 19 since their sand fraction is not available. Nevertheless, for sandy soil named "Sable de Rivière", in particular, it is highly likely that the sand fraction and porosity fraction associated with macropores (equal to 85%) are comparable to each other.

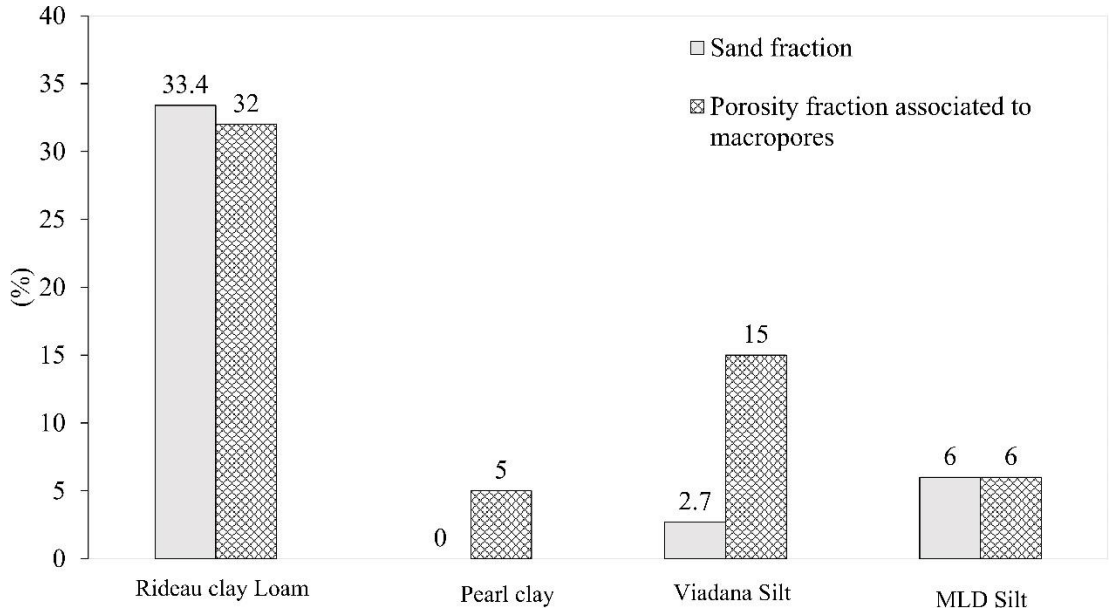

Fig. 19. Comparison between sand fraction and simulated porosity fraction associated to macropores

5.2.2.4. Calibration of the critical radius r_{cr}

As detailed in section 4, the critical radius r_{cr} is a calibration parameter that can be interpreted as the radius below which pores feature is more oblong than a cylindrical shape. In other words, it could be the threshold between capillary and C–S–H pores. For soils, it is more appropriate to define critical radius as the threshold between macropores and micropores. Nevertheless, as seen in Table 2, the value of r_{cr} varies from one soil to another while it remained constant for cement-based materials (Ranaivomanana et al. 2011, 2013). Such difference is obviously due to the diversity in soil structure, making the relevant estimation of r_{cr} complex for a given type of soil. Despite this complexity, an interesting correlation can be

established between the clay fraction and the ratio between the mode value of macropores denoted as $r_{macropores,}$ and the critical radius r_{cr}. Indeed, it would appear in Fig. 20 that $r_{macropores}/r_{cr}$ ratio decreases exponentially with the increase of clay fraction. Given that the value of $r_{macropores}$ can be obtained from MIP test as discussed in section 5.2.2.1, the corresponding value of critical radius can thus, as a first approximation, be estimated using the following relationship given by Eq. 7.

$$r_{cr} = \frac{r_{macropores}}{10106 f^{-2.133}} \quad (7)$$

where f is the clay fraction.

It is worth noting that the unknown clay fraction of loamy soil named "Touchet Silt loam" was estimated to be in the range of 20 to 40% based on soil textural classes defined by Survey (1993). On the other hand, the sandy soil named "Sable de Rivière" was not represented in Fig. 20 since the $r_{macropores}/r_{cr}$ ratio equal to 0.53 was found, despite a low clay fraction (estimated to be less than 15%). Such a result is probably the consequence of a more pronounced influence of the granular structure of sandy soils on the shapes of pores compared to that of the clay fraction. Of course, further investigations are necessary for the purpose of a better understanding and a more relevant prediction of the evolution of critical radius depending on the type of soil.

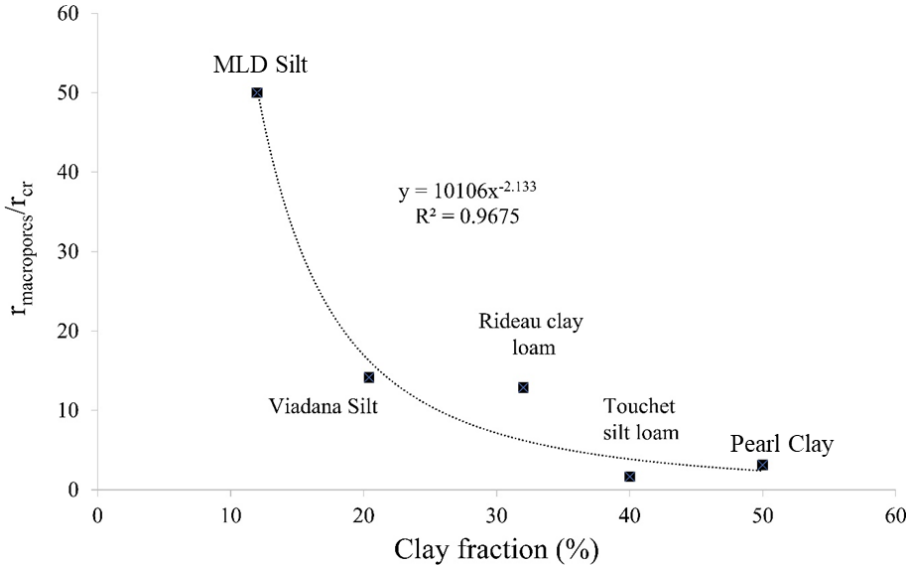

520

521

522 **Fig. 20.** Evolution of $r_{macropores}/r_{cr}$ ratio vs. clay fraction

523 A flowchart that explains the main inputs and the main procedures to calculate intermediate
524 variables including radius, amplitude and height of porous modes for the obtention of SWRC is presented
525 in Fig. 21.

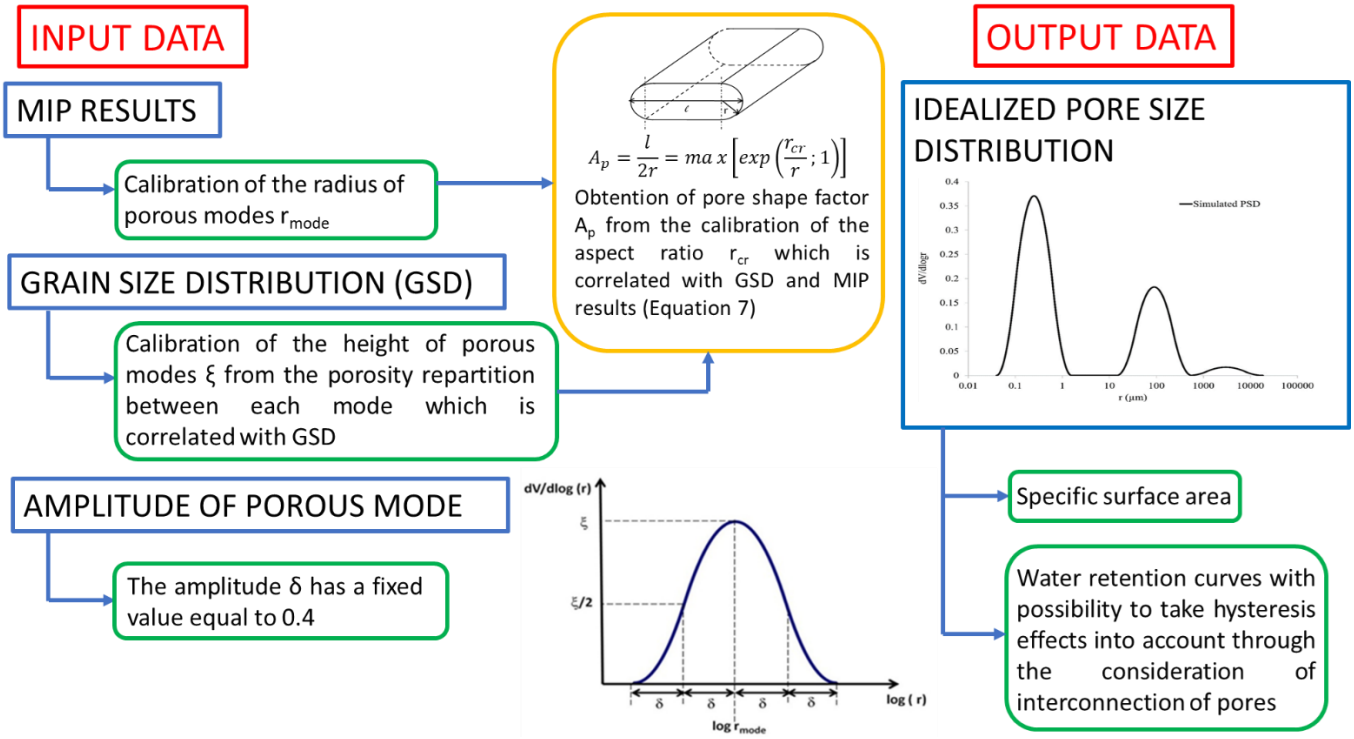

Fig. 21. Flowchart explaining the main inputs and the main procedures to calculate intermediate variables for the obtention of SWRC

6. Conclusion

A physical porous network model has been developed for soils to simulate SWRC and to predict any hysteresis. The modeling was based on a pore size distribution previously developed for cementitious materials. The model takes into account in an accurate way the double porosity encountered in soils and was also able to predict the specific surface area of soils. Each porous mode of the pore size distribution is characterized by 3 parameters: the mode radius, its amplitude δ, and its height ξ. The mode values can be obtained from MIP test while the value of δ was fixed at 0.4 (in log(r), where r is in nm). The height of a porous mode was computed from the porosity associated with each mode by assuming that the porosity fraction related to inter-aggregates macropores corresponds to a sand fraction while that related to intra-aggregates micropores corresponds to a fine fraction.

Similarly, to cementitious materials, a function of inter-connectivity was associated with the pore size distribution to manage the hysteresis attributed to ink-bottle effects. The inter-connectivity was approximated by the ratio between the total length of pores affected by drying at a given pore suction and the total cumulative length of all pores of the network. For that purpose, small pores were represented with an oblong geometry characterized by a progressive dimension's ratio managed by an aspect ratio involving a parameter noted r_{cr} (critical radius). For soils, the critical radius can be defined as the transition size between macropores with cylindrical shape and micropores with oblong shape. As a first approximation, r_{cr} has been correlated with the clay fraction and the mode value of macropores. Nevertheless, further investigations are necessary to achieve a better understanding of the evolution of this parameter depending on the type of soil since the shape of pores is not influenced only by the clay fraction but also by the granular structure.

The simulations, performed on different types of soils, allow reproducing SWRC satisfactorily with hysteresis loops. The next step is to extend the model to predict the evolution of pore structure under thermo-hydro-chemo-mechanical loadings and their effects on SWRC and other properties like permeability and diffusivity.

7. References

Abbasi, F., Javaux, M., Vanclooster, M., Feyen, J.: Estimating hysteresis in the soil water retention curve from monolith experiments. Geoderma. 189, 480-490 (2012). https://doi.org/10.1016/j.geoderma.2012.06.013

Al-Mukhtar, M., Belanteur, N., Tessier, D., Vanapalli, S.K. : The fabric of a clay soil under controlled mechanical and hydraulic stress states. Applied Clay Science. 11, 99–115 (1996). https://doi.org/10.1016/S0169-1317(96)00023-3

Assouline, S., Tessier, D., Bruand, A.: A conceptual model of the soil water retention curve. Water Resources Research. 34, 223–231(1998). https://doi.org/10.1029/97WR03039

ASTM, D.: Standard test methods for laboratory determination of water (moisture) content of soil and rock by mass. Annual Book of ASTM Standards (2010).

Azizi, A., Jommi, C., Musso, G.: A water retention model accounting for the hysteresis induced by hydraulic and mechanical wetting-drying cycles. Computers and Geotechnics. 87, 86–98 (2017). https://doi.org/10.1016/j.compgeo.2017.02.003

Barast, G., Razakamanantsoa, A.-R., Djeran-Maigre, I., Nicholson, T., Williams, D.: Swelling properties of natural and modified bentonites by rheological description. Applied Clay Science. 142, 60–68 (2017). http://dx.doi.org/10.1016/J.clay.2016.01.008

Barrett, E.P., Joyner, L.G., Halenda, P.P.: The determination of pore volume and area distributions in porous substances. I. Computations from nitrogen isotherms. Journal of the American Chemical society. 73, 373–380 (1951). https://doi.org/10.1021/ja01145a126

Bear, J.: Dynamics of fluids in porous media. Courier Corporation (2013).

Beckett, C.T.S., Augarde, C.E.: Prediction of soil water retention properties using pore-size distribution and porosity. Canadian Geotechnical Journal. 50, 435–450 (2013). https://doi.org/10.1139/cgj-2012-0320

Brunauer, S., Emmett, P.H., Teller, E.: Adsorption of gases in multimolecular layers. Journal of the American chemical society. 60, 309–319 (1938). https://doi.org/10.1021/ja01269a023

Carsel, R.F., Parrish, R.S.: Developing joint probability distributions of soil water retention characteristics. Water resources research. 24, 755–769 (1988). https://doi.org/10.1029/WR024i005p00755

Casini, F., Vaunat, J., Romero, E., Desideri, A. : Consequences on water retention properties of double-porosity features in a compacted silt. Acta Geotechnica. 7, 139–150 (2012).

Chen, P., Lu, N., Wei, C.: General Scanning Hysteresis Model for Soil–Water Retention Curves. Journal of Geotechnical and Geoenvironmental Engineering. 145, 04019116 (2019). 10.1061/(ASCE)GT.1943-5606.0002184

Chen, P., Wei, C., Ma, T.: Analytical model of soil-water characteristics considering the effect of air entrapment. International Journal of Geomechanics. 15, 04014102 (2015). https://doi.org/10.1061/(ASCE)GM.1943-5622

Cheng, Q., Ng, C.W.W., Zhou, C., Tang, C.-S.: A new water retention model that considers pore non-uniformity and evolution of pore size distribution. Bulletin of Engineering Geology and the Environment. 78, 5055–5065 (2019). https://doi.org/10.1007/s10064-019-01476-4

Soil Science Glossary Terms Committee, Soil Science Society of America. Glossary of soil science terms 2008. ASA-CSSA-SSSA (2008).Coulon, E., Bruand, A.: Effects of compaction on the pore space geometry in sandy soils. Soil and Tillage Research. 15, 137–151 (1989).

Cuisinier, O., Laloui, L.: Fabric evolution during hydromechanical loading of a compacted silt. International Journal for Numerical and Analytical Methods in Geomechanics. 28, 483–499 (2004).

Dane, J.H., Wierenga, P.J.: Effect of hysteresis on the prediction of infiltration, redistribution and drainage of water in a layered soil. Journal of Hydrology. 25, 229–242 (1975). https://doi.org/10.1016/0022-1694(75)90023-2

Das, G., Razakamanantsoa, A., Herrier, G., Saussaye, L., Lesueur, D., Deneele, D.: Evaluation of the long-term effect of lime treatment on a silty soil embankment after seven years of atmospheric exposure: Mechanical, physicochemical, and microstructural studies. Engineering Geology. 281, 105986 (2020). https://doi.org/10.1016/j.enggeo.2020.105986

Das, G., Razakamanantsoa, A., Herrier, G., Deneele, D.: Compressive strength and microstructure evolution of lime-treated silty soil subjected to kneading action. Transportation Geotechnics. 29, 100568 (2021). https://doi.org/10.1016/j.trgeo.2021.100568

de la Morena, G., Navarro, V., Asensio, L., Gallipoli, D.: A water retention model accounting for void ratio changes in double porosity clays. Acta Geotechnica. 1–16 (2021). https://doi.org/10.1007/s11440-020-01126-0

Delage, P., Cui, Y.J. : L'eau dans les sols non saturés, techniques de l'ingénieur, in: Traité Construction, C301 (2000).

Delage, P., Lefebvre, G.: Study of the structure of a sensitive Champlain clay and of its evolution during consolidation. Canadian Geotechnical Journal. 21, 21–35 (1984). https://doi.org/10.1139/t84-003

Durner, W.: Hydraulic conductivity estimation for soils with heterogeneous pore structure. Water resources research. 30, 211–223 (1994). https://doi.org/10.1029/93WR02676

Espinal, L.: Porosity and its measurement. Characterization of Materials. 1–10 (2002). https://doi.org/10.1002/0471266965.com129

622 Feng, M., Fredlund, D.G.: Hysteretic influence associated with thermal conductivity sensor measurements,
623 in: Proceedings from Theory to the Practice of Unsaturated Soil Mechanics in Association with the
624 52nd Canadian Geotechnical Conference and the Unsaturated Soil Group, Regina, Sask. pp. 14–20
625 (1999).

626 Gapak, Y., Das, G., Yerramshetty, U., Bharat, T.V.: Laboratory determination of volumetric shrinkage
627 behavior of bentonites: A critical appraisal. Applied Clay Science. 135 (2017).
628 https://doi.org/10.1016/j.clay.2016.10.038

629 Griffiths, F.J., Joshi, R.C. Change in pore size distribution due to consolidation of clays. Geotechnique. 39,
630 159–167 (1989). https://doi.org/10.1680/geot.1989.39.1.159

631 Han, Z., Vanapalli, S.K., Zou, W. : Simple Approaches for Modeling Hysteretic Soil Water Retention
632 Behavior. Journal of Geotechnical and Geoenvironmental Engineering. 145, 04019064 (2019).
633 https://doi.org/10.1061/(ASCE)GT.1943-5606.0002148

634 Haverkamp, R., Bouraoui, F., Zammit, C., Angulo-Jaramillo, R.: Soil properties and moisture movement
635 in the unsaturated zone. The handbook of groundwater engineering (1998).

636 Hayashida, Y., Kohgo, Y., Asano, I.: A hysteresis model with continuity of tangential slopes of soil–water
637 retention curves, in: Proceedings of the 2nd Asian Conference on Unsaturated Soils, Osaka, Japan.
638 pp. 325–333 (2003).

639 Hu, R., Chen, Y.-F., Liu, H.-H., Zhou, C.-B.: A water retention curve and unsaturated hydraulic
640 conductivity model for deformable soils: consideration of the change in pore-size distribution.
641 Géotechnique. 63, 1389–1405 (2013). https://doi.org/10.1680/geot.12.P.182

642 Jackson, R.D., Reginato, R.J., van Bavel, C.H.M.: Comparison of measured and calculated hydraulic
643 conductivities of unsaturated soils. Water resources research. 1, 375–380 (1965).
644 https://doi.org/10.1029/WR001i003p00375

645 Jensen, M.E., Hanks, R.J.: Nonsteady-state drainage from porous media. Proceedings of the American
646 Society of Civil Engineers, Journal of the Irrigation and Drainage Division. 93, 209–231 (1967).

647 Juang, C.H., Lovell, C.W.: Measurement of Pore-Size Density Function in Sand. Transportation Research
648 Record (1986).

649 Karube, D., Kawai, K.: The role of pore water in the mechanical behavior of unsaturated soils. Geotechnical
650 & Geological Engineering. 19, 211–241 (2001). https://doi.org/10.1023/A:1013188200053

651 Kawai K, Kato S, Karube D.: The model of water retention curve considering effects of void ratio.
652 InUnsaturated soils for Asia Sep 10 (pp. 329-334) (2000). CRC Press.Klausner, Y.: Fundamentals of
653 continuum mechanics of soils. Springer Science & Business Media (2012).

654 Klobes, P., Munro, R.G.: Porosity and specific surface area measurements for solid materials (2006).

655 Kuila, U., Prasad, M.: Specific surface area and pore-size distribution in clays and shales. Geophysical
656 Prospecting. 61, 341–362 (2013). https://doi.org/10.1111/1365-2478.12028

657 Li, X., Zhang, L.M. : Characterization of dual-structure pore-size distribution of soil. Canadian
658 geotechnical journal. 46, 129–141(2009). https://doi.org/10.1139/T08-110

659 Likos, W.J., Lu, N., Godt, J.W.: Hysteresis and uncertainty in soil water-retention curve parameters. Journal
660 of Geotechnical and Geoenvironmental Engineering. 140, 04013050 (2014).
661 https://doi.org/10.1061/(ASCE)GT.1943-5606.0001071

662 Liu, Z., Yu, B., Wan-Wendner, L., : An investigation in the influence of contact angle on Soil Water
663 Characteristic Curve with a modified capillary rise method. Transportation Research Record Journal
664 of the Transportation Research Board. (2349), 32-40 (2013).

665 Mindess, S., Young, J.F., Darwin, D.: *Concrete*, 2nd edition Prentice Hall, Englewood Cliffs, NJ (2002).

666 Nimmo, J.R.: Semiempirical model of soil water hysteresis. Soil Science Society of America Journal. 56,
667 1723–1730 (1992). https://doi.org/10.2136/sssaj1992.03615995005600060011x

668 Oualmakran, M., Mercatoris, B.C.N., François, B. : Pore-size distribution of a compacted silty soil after
669 compaction, saturation, and loading. Canadian Geotechnical Journal. 53, 1902–1909 (2016).
670 https://doi.org/10.1139/cgj-2016-0184

671 Pham, H.Q., Fredlund, D.G., Barbour, S.L.: A study of hysteresis models for soil-water characteristic
672 curves. Canadian Geotechnical Journal. 42, 1548–1568 (2005). https://doi.org/10.1139/t05-071

673 Prapaharan, S., Altschaeffl, A.G., Dempsey, B.J.: Moisture curve of compacted clay: mercury intrusion
674 method. Journal of Geotechnical Engineering. 111, 1139–1143 (1985).
675 https://doi.org/10.1061/(ASCE)0733-9410(1985)111:9(1139)

676 Rahardjo, H., Aung, K.K., Leong, E.C., Rezaur, R.B.: Characteristics of residual soils in Singapore as
677 formed by weathering. Engineering Geology. 73, 157–169 (2004).
678 https://doi.org/10.1016/j.enggeo.2004.01.002

679 Ranaivomanana, H., Razakamanantsoa, A., Amiri, O.: Effects of cement treatment on microstructural,
680 hydraulic, and mechanical properties of compacted soils: Characterization and modeling. International
681 Journal of Geomechanics. 18, 04018106 (2018). https://doi.org/10.1061/(ASCE)GM.1943-
682 5622.0001248

683 Ranaivomanana, H., Razakamanantsoa, A., Amiri, O.: Permeability prediction of soils including degree of
684 compaction and microstructure. International Journal of Geomechanics. 17, 04016107 (2017).
685 https://doi.org/10.1061/(ASCE)GM.1943-5622.0000792

686 Ranaivomanana, H., Verdier, J., Sellier, A., Bourbon, X. Prediction of relative permeabilities and water
687 vapor diffusion reduction factor for cement-based materials. Cement and Concrete Research. 48, 53–
688 63 (2013). https://doi.org/10.1016/j.cemconres.2013.02.008

689 Ranaivomanana, H., Verdier, J., Sellier, A., Bourbon, X. : Toward a better comprehension and modeling
690 of hysteresis cycles in the water sorption–desorption process for cement based materials. Cement and
691 Concrete Research. 41, 817–827 (2011). https://doi.org/10.1016/j.cemconres.2011.03.012

692 Ranaivomanana, H. : Transferts dans les milieux poreux réactifs non saturés: application à la cicatrisation
693 de fissure dans les matériaux cimentaires par carbonatation, *PhD Thesis*, Université de Toulouse (in
694 French) (2010).

695 Romero, E., Gens, A., Lloret, A. : Water permeability, water retention and microstructure of unsaturated
696 compacted Boom clay. Engineering Geology. 54, 117–127 (1999). https://doi.org/10.1016/S0013-
697 7952(99)00067-8

698 Russell, A.R.: Water retention characteristics of soils with double porosity. European Journal of Soil
699 Science. 61, 412–424. https://doi.org/10.1111/j.1365-2389.2010.01237.xSatyanaga, A., Rahardjo, H.,
700 Leong, E.-C., Wang, J.-Y., 2013. Water characteristic curve of soil with bimodal grain-size
701 distribution. Computers and Geotechnics. 48, 51–61 (2010).
702 https://doi.org/10.1016/j.compgeo.2012.09.008

703 Scott, P.S.: Hysteretic effects on net infiltration. Advances in infiltration. 163–170 (1983).

704 Simms, P.H., Yanful, E.K.: Predicting soil—water characteristic curves of compacted plastic soils from
705 measured pore-size distributions. Géotechnique. 52, 269–278 (2002).
706 https://doi.org/10.1680/geot.2002.52.4.269

Simms, P.H., Yanful, E.K. : Measurement and estimation of pore shrinkage and pore distribution in a clayey till during soil-water characteristic curve tests. Canadian Geotechnical Journal. 38, 741–754 (2001). https://doi.org/10.1139/t01-014

Sumner, M.E.: Handbook of soil science. CRC press (1999).

Sun, D.A., Sheng, D.C., Cui, H.B., Sloan, S.W.: A density-dependent elastoplastic hydro-mechanical model for unsaturated compacted soils. International journal for numerical and analytical methods in geomechanics. 31, 1257–1279 (2007). https://doi.org/10.1002/nag.579

Sun, W-J., Cui, Y-J.: Determining the soil-water retention curves using mercury intrusion porosimetry test in consideration of soil volume change. Journal of Rock Mechanics and Geotechnical Engineering. 12 (5), 1070-1079 (2020).

Survey, U.States.D. of S.: Soil survey manual. US Department of Agriculture (1993).

Tarantino, A.: A water retention model for deformable soils. Géotechnique 59, 751–762 (2009). https://doi.org/10.1680/geot.7.00118

Topp, G.C.: Soil-water hysteresis: The domain theory extended to pore interaction conditions. Soil Science Society of America Journal. 35, 219–225 (1971). https://doi.org/10.2136/sssaj1971.03615995003500020017x

Toride, N., Sakai, M., Šimůnek, J. A hysteretic model of hydraulic properties for dual-porosity soils. Soil Science Society of America Journal. 77, 1182–1188 (2013). https://doi.org/10.2136/sssaj2012.0339n

Vachaud, G. : Vérification de la loi de Darcy généralisée et détermination de la conductivité capillaire à partir d'une infiltration horizontale. International Association of Hydrological Sciences. 82, 277–292 (1966).

Wheeler, S.J., Sharma, R.S., Buisson, M.S.R.: Coupling of hydraulic hysteresis and stress–strain behaviour in unsaturated soils. Géotechnique. 53, 41–54 (2003). https://doi.org/10.1680/geot.2003.53.1.41

Wijaya, M., Leong, E.C. Equation for unimodal and bimodal soil–water characteristic curves. Soils and Foundations. 56, 291–300 (2016). https://doi.org/10.1016/j.sandf.2016.02.011

Zhai, Q., Rahardjo, H., Satyanaga A., Dai, G.: Estimation of the soil water characteristic curve from the grain size distribution of coarse-grained soils. Engineering Geology. 267, 105502 (2020).